

1 **Intermittent upwelling events trigger delayed, major,**
2 **and reproducible pico-nanophytoplankton responses in**
3 **coastal oligotrophic waters**

4 **R. Fuchs^{1,2*}, V. Rossi^{2†}, C. Caille^{3‡},**
5 **N. Bensoussan^{2§}, C. Pinazo^{2¶}, O. Grosso^{2||}, M. Thyssen^{2**}**

6 ¹Aix Marseille Univ, CNRS, Centrale Marseille, I2M, Marseille, France
7 ²Aix Marseille Univ, Université de Toulon, CNRS, IRD, MIO, Marseille, France
8 ³Sorbonne Université, CNRS, LOMIC, Banyuls-sur-Mer, France

9 **Key Points:**

- 10 • Biomass peaks and daily rates of increase induced by the most extreme upwellings
11 are of the same magnitude as the spring bloom ones.
12 • Phytoplankton abundance/biomass reactions start less than 2 days/4 days after
13 the upwelling onset and last 2 to 5 days.
14 • During upwelling events all biomasses (but *Synechococcus*) median/maximum in-
15 creases range 50-173/100-400%, then sharply drop back to normal.

*robin.fuchs@univ-amu.fr

†vincent.rossi@mio.osupytheas.fr

‡caillec@obs-banyuls.fr

§nathaniel.bensoussan@mio.osupytheas.fr

¶christel.pinazo@mio.osupytheas.fr

||olivier.grosso@mio.osupytheas.fr

**melilotus.thyssen@mio.osupytheas.fr

Corresponding author: Melilotus Thyssen, melilotus.thyssen@mio.osupytheas.fr

Abstract

Pico-nanophytoplankton organisms are dominant in oceanic oligotrophic areas but their highly adaptive growth rates make their contribution to the carbon cycle difficult to estimate. Here we address the response capacities of these microorganisms after intermittent wind gusts causing sporadic upwelling events in a coastal Mediterranean station. When the water column is stratified, corresponding to oligotrophic conditions, these events generate intense short-lived nutrient pulses and seawater temperature drops lasting six days on average with decreases up to -10°C . Using a flow cytometer and statistical rupture-detection methods, we characterize the responses of five pico-nanophytoplankton functional groups at a two-hour frequency from September 2019 to November 2021. These events trigger delayed increases in both abundances and biomasses for most groups that can overpass spring bloom values, and are immediately followed by an overall decrease, suggesting a clear physical driver. These submesoscale events could significantly influence coastal carbon budgets if not included.

Plain Language Summary

Short-lived north-westerlies in the Mediterranean sea replace surface coastal waters with colder and potentially richer in nutrients deeper waters from offshore. This phenomenon, called a sporadic upwelling event, lasts only a few days after the wind stops and induces brutal environmental shifts. During summer, upwellings generate drops in surface water temperature of up to 10°C and are expected to impact significantly phytoplankton. Small phytoplankton are conspicuous for their fast response to environmental changes thanks to their high division rates (up to several times a day). As a result, the biological response to wind-induced upwellings has to be studied using high-frequency measurements. Using four attributes for each of the five studied phytoplankton groups, we show that the number of cells of most groups rose strongly in less than two days after the temperature drop according to remarkable repeatable patterns. Similarly, total biomass increased after less than four days. The reactions themselves lasted up to five days before going back near to the initial level. Brought back to a daily scale, the described phytoplankton reactions to local upwelling events can be as important as the ones observed during the spring bloom, regarded as the most important annual event.

1 Introduction

Coastal zones play a significant role in the global carbon cycle as they sustain, despite large uncertainties, up to 30% of the global oceanic primary production (Gattuso et al., 1998). Previous research suggested the importance of taking into account the diversity and variability of near-shore ecosystems, which remain poorly known and under the influences of complex physical forcing (Borges et al., 2005; Bauer et al., 2013; Wimart-Rousseau et al., 2020) that strongly shapes phytoplankton communities (Morel & André, 1991; Antoine et al., 1995; Bosc et al., 2004; Armbrrecht et al., 2014), themselves responsible for near the half of the world primary production (Field et al., 1998). Furthermore, there is evidence of the fast response capacities of phytoplankton after environmental changes, notably considering the prominence of meso and submesoscale processes in the ocean (Lévy et al., 2012). This is especially true for the pico-nanophytoplankton cells that present adaptive growth rates enhancing their competitive strategies (Lomas et al., 2009). The pico-nanophytoplankton size class is composed of polyphyletic unicellular photosynthetic microorganisms that dominate primary production in oligotrophic basins (Li, 1995; Grob et al., 2007) and are numerically dominant in less oligotrophic conditions outside of the main spring and autumn bloom periods (Bolaños et al., 2020). They contribute substantially to the export of organic carbon into the deep layers mainly by aggregation or via grazing and subsequent sinking of organic materials (Richardson & Jackson, 2007; Lomas & Moran, 2011).

66 To assess the typical speed and frequency of community shifts that inform the ca-
67 pacity of pico-nanophytoplankton adaptation to abrupt changes in their environment,
68 long-term and high-frequency sampling strategies allowing the separation of phytoplank-
69 ton cells into functionally meaningful size classes are required. Martin-Platero et al. (2018)
70 relied on a time series composed of daily samples for 93 days to show that physical forc-
71 ing strongly shapes phytoplankton communities and that the observed patterns were highly
72 dependent on the sampling frequency. Similarly, Martiny et al. (2016) have demonstrated
73 some significant correlations of cyanobacteria, pico and nanoeukaryotes abundances with
74 temperature as well as nutrients using weekly samples over three years. Hunter-Cevera
75 et al. (2020) used a 16-year long time series at an hourly frequency to highlight the sea-
76 sonal cycles of *Synechococcus* abundances and proposed an explanation for *Synechococ-*
77 *cus* blooms relying on growth rates variations. Wilkerson et al. (2006) demonstrated that
78 wind-induced upwelling events followed by relaxation periods trigger optimal growth con-
79 ditions for phytoplankton cells, depleting the upwelled nutrients and fostering a commu-
80 nity of large phytoplanktonic cells (e.g. large diatoms), in line with Rossi et al. (2013).
81 In more oligotrophic coastal areas, the responses of phytoplanktonic communities to short-
82 lived enrichment events are more puzzling (Armbrecht et al., 2014) and suggest these fa-
83 vor rather the small-sized phytoplanktonic cells. Thyssen et al. (2008) and Dugenne et
84 al. (2014) have indeed shown important responses of pico-nanophytoplankton groups af-
85 ter strong north-westerlies events in the Bay of Marseille. Apart from atmospheric or
86 riverine inputs and other classes of submesoscale frontal dynamics, sporadic wind-driven
87 upwelling events are one major source of nutrients in the surface layers of various olig-
88 otrophic coastal areas (Milot, 1979; Bakun & Agostini, 2001; Palma & Matano, 2009;
89 Rossi et al., 2014). While their hydrographic impacts, temperature cooling and nutri-
90 ent enrichment of surface waters, are relatively well documented, little information ex-
91 ists on how they influence phytoplankton communities at hourly scales and functional group
92 resolution. The Bay of Marseille constitutes a natural laboratory to study the biolog-
93 ical impacts of such events since they are common and frequent during stratified sum-
94 mer periods (\sim three events/month in stratified period according to Odic et al. (2022)).

95 To our knowledge, all previous studies did not focus on wind events exclusively (Martiny
96 et al., 2016; Hunter-Cevera et al., 2020), had low statistical power (Thyssen et al., 2008;
97 Dugenne et al., 2014; Martin-Platero et al., 2018), had an insufficient temporal resolu-
98 tion (daily frequency for Wilkerson et al. (2006), weekly frequency in Martiny et al. (2016))
99 or did not fully resolve the pico-nanophytoplankton size class (Wilkerson et al., 2006;
100 García-Reyes et al., 2014; Hunter-Cevera et al., 2020). In this study, we analyzed twenty
101 short-lived wind-driven events occurring when the water column was stratified (late spring,
102 summer, and early fall) allowing the detection of clear upwelling signatures in compar-
103 ison to unstratified periods. The causal effect of the physical forcing was identified us-
104 ing a bi-hourly time series capturing the dynamics of five phytoplankton functional groups
105 as resolved by Automated Flow Cytometry (Dubelaar & Gerritzen, 2000; Olson et al.,
106 2003) over two complete years. The area of interest is the French Bay of Marseille, which
107 is considered oligotrophic in stratified periods during which it is generally affected by
108 the regional offshore bloom occurring in winter-early spring and fall seasons (d’Ortenzio
109 & Ribera d’Alcalà, 2009). It is dominated by pico-nanophytoplankton size classes and
110 its hydrology is strongly influenced by North-westerlies winds generating regularly short-
111 lived upwelling events (Bensoussan et al., 2010; Pairaud et al., 2011; Fraysse et al., 2013;
112 Lajaunie-Salla et al., 2021; Odic et al., 2022).

113 2 Materials and Methods

114 The temperature, nutrients, and phytoplankton data were collected from Septem-
115 ber 19, 2019, to November 31, 2021, at the Sea Water Sensing Laboratory @ MIO Mar-
116 seille (SSL@MM), a coastal marine station in the North-West Mediterranean Sea (43°17’
117 N, 5°22’ E). Seawater was continuously pumped at 10 meters from the coastline at a depth

of 3 meters (with a seabed at 5 meters deep) and delivered into the laboratory using a VerderFlex 40 peristaltic pump. The seawater was coarsely pre-filtered by a PVC strainer (3 mm) and routed by polypropylene pipes that are cleaned monthly.

The temperature data were acquired every hour using an STPS sensor from the NKE-manufacturer presenting a temperature accuracy of 0.05°C. Nutrient samples were collected every four days on average and stored at -20°C until they were analyzed in a laboratory using a Technicon Autoanalyser® (SEAL Analytical) as in Tréguer and Le Corre (1975).

2.1 Phytoplankton Acquisition by Automated Pulse-shape Recording Flow Cytometry

Phytoplankton data were sampled every two hours using an Automated pulse-shape recording Flow Cytometer (Dubelaar et al., 1999; Dubelaar & Gerritzen, 2000) with the same protocol as in Marrec et al. (2018). We relied on the nomenclature proposed by Thyssen et al. (2021) (<http://vocab.nerc.ac.uk/collection/F02/current/>) and resolved five cytometric phytoplankton functional groups (PFGs): Redpicopro, Orgpicopro, Redpicoeuk, Rednano, and Orgnano, which were previously often referred to as *Prochlorococcus*, *Synechococcus*, picoeukaryotes, nanoeukaryotes, and cryptophytes, respectively. Microphytoplankton cells were collected but were not representative enough to be reported here: 75% of the samples presented less than 13 particles per milliliter. Each cell was assigned to a PFG by a Convolutional Neural Network (CNN) introduced in Fuchs et al. (2022).

2.2 Phytoplankton Biovolume, Biomass, and Growth Rate Estimations

Biovolume and biomass were estimated through empirical relationships (see Figure S1, sections 1.2 and 1.3 in Supplemental Information) following Verity et al. (1992), Menden-Deuer and Lessard (2000), Sun and Liu (2003) and Marrec et al. (2018). The functional groups growth rate was estimated from the cell biovolumes (see Table S1 in Supplemental Information) using a size-structured population model introduced by Sosik et al. (2003) and adapted by Ribalet et al. (2015).

2.3 Wind-driven Upwelling Signatures

The occurrence and strength of each upwelling event were assessed based on the positive values of the Wind-driven Upwelling/Downwelling Index (WUDI) developed and extensively validated by Odic et al. (2022) following Bakun (1973). The drop in temperature generated during an upwelling-favorable wind was evaluated as the difference between the measured water temperature and its low-pass filtered time series using a cut-off frequency of 15 days as in Rossi et al. (2014) and Odic et al. (2022) (Figure 1 a). These temperature drops, or anomalies, were used to delimit three physical phases: (i) a pre-anomaly phase when the water temperature is stable and high, (ii) an anomaly phase when the temperature drops, stays cool for a few hours/days to then warm-up slowly, and (iii) a post-anomaly phase when the temperature has returned to a warmer and more stable state. These anomalies are particularly significant during the summer when the water column is stratified. A period was considered stratified when the filtered temperature was higher than the annual average temperature and conversely for unstratified periods as in Odic et al. (2022). Among the 54 events recorded over two years, only 20 events occurred during stratified periods and had temperature and flow cytometry data available. Besides, all successive events marked with negative seawater temperature anomalies separated by less than one day were not considered in order to have for each event a minimal relaxation time. In other words, we retain here only the significant wind-driven events happening in stratified periods that are surrounded by relatively calm periods, denoted "Stratified period Wind-induced Upwelling Event", SWUE.

167 The spring blooms occurring in unstratified periods were used to benchmark the
 168 biomass (and abundance) increases generated by SWUEs as the spring blooms are ex-
 169 pected to be the most productive periods (Fraysse et al., 2013). The bloom dates were
 170 determined using the threshold method (Sapiano et al., 2012; Brody et al., 2013) and
 171 the median biomass and abundance per PFG during the bloom were used as the refer-
 172 ence benchmark level (see section S1.5 in Supplemental Information). The biomass in-
 173 crease imputable to the blooms was computed using the median biomass during the week
 174 preceding the bloom as a reference value.

175 **2.4 Rupture Detection and Response Characterization**

176 The biological response of each PFG to the SWUE was evaluated in terms of both
 177 abundances and biomasses using a statistically-based rupture detection method presented
 178 in Truong et al. (2020). This mathematically well-founded method looked for ruptures
 179 in causal time series. It is here employed to detect potential changes in the link exist-
 180 ing between the temperature signal and each PFG abundance or biomass. The link was
 181 here assumed to be linear (Bai & Perron, 2003) and rupture detections were performed
 182 on biomasses and abundances separately. This methodology encompasses the idea that
 183 PFGs respond to a change in their environment, and delimited the start and end of the
 184 reactions for each PFG. The response of each PFG is hence composed of three phases:
 185 a pre-reaction, a reaction, and a post-reaction phase (called the relaxation phase).

186 Based on the identified ruptures, four key variables per PFG were used to charac-
 187 terize the duration and magnitude of the biological responses as presented in Figure 2
 188 a). The reaction delay is the time taken by a PFG to react after the rise of physical forc-
 189 ing, i.e. between the start of the water cooling and the beginning of the PFG automati-
 190 cally identified reaction. The reaction duration measures the length of the reaction phase.
 191 The reaction and relaxation magnitudes are computed as the difference in medians dur-
 192 ing the pre-reaction and reaction phases and during the reaction and relaxation phases,
 193 respectively. To capture only PFGs causal responses to sporadic upwelling events, only
 194 the PFG responses for which the reactions occurred after the beginning of the anomaly
 195 phase were considered, which was the case for most events and PFGs. The number of
 196 SWUEs taken into account for each PFG is given in Figure 3.

197 More material and method details are given in Supplemental Information (section 1 and
 198 Figure S2).

199 **3 Results**

200 **3.1 Seawater Temperature and Nutrients as Markers of Sporadic Up- 201 welling Events**

202 The annual mean temperature over the three years was 17.8°C in 2019, 17.1°C in
 203 2020, and 17.3°C in 2021. The associated stratified periods started on May, 8 in 2020,
 204 and May, 25 in 2021 (not available in 2019), and ended on November, 13 in 2019, Oc-
 205 tober, 27 in 2020, and October, 31 in 2021. The number of significant and distinct SWUEs
 206 during the stratified periods was two in 2019, ten in 2020, and eight in 2021. The me-
 207 dian duration anomaly phase of the SWUEs was of six days and the subsequent drops
 208 in water temperature (difference between both maximal and minimal values recorded dur-
 209 ing each SWUE) varied from 0.7°C to 9.9°C, with a median value of 4.7°C (see also Odic
 210 et al. (2022)).

211 Nutrient concentrations and N/P ratio were higher during unstratified periods as
 212 compared to stratified periods, except for phosphate concentration (Figure S3 in Sup-
 213 plemental Information; Kruskal-Wallis test, p-value $\leq 1.0E-7$ for nitrites, nitrates, and
 214 N/P ratio, p-value ≤ 0.05 for ammonium). In stratified periods, the nitrite concentra-

215 tion and N/P ratios were higher and nitrate concentration lower during SWUEs than
 216 outside the SWUEs. The concentrations of phosphate and ammonium were however com-
 217 parable during and outside the SWUEs. The N/P ratio was 25.15 in the unstratified pe-
 218 riod, 17.33 during SWUEs, and 13.05 in the stratified period outside of the SWUEs. Yet,
 219 only the nitrite concentrations recorded during and outside SWUEs under stratified con-
 220 ditions were significantly different (Kruskal-Wallis test, p -value = 0.034). The concen-
 221 trations are given in Tables S2 and S3 in Supplemental Information.

222 3.2 Wind-induced Upwelling Events Trigger Peaks of Biomass and Abun- 223 dances

224 All SWUEs triggered noticeable peaks of biomass for most PFGs (Figure 1 and Fig-
 225 ure S4 in Supplemental Information). The pico-nanophytoplankton biomass was domi-
 226 nated in both stratification regimes by Rednano cells, followed by Orgnano, Orgpicopro,
 227 Redpicoeuk, and Redpicopro cells (Table S4 in Supplemental Information). Orgnano
 228 exceeded their median bloom biomass during one-third of the SWUEs (Table S5 in Sup-
 229 plemental Information). Similarly, more than half of the Orgpicopro and Rednano peaks
 230 went over their median bloom values. Finally, Redpicoeuk and Redpicopro biomass peak
 231 values were higher than their median bloom values in 4/5 SWUEs and all SWUEs, re-
 232 spectively.

233 In terms of abundance, the SWUEs generated peaks for most PFGs (Figure S5 in
 234 Supplemental Information). Over the whole series, the most abundant PFGs were the
 235 Orgpicopro, followed by the Redpicopro, Redpicoeuk, Rednano, and Orgnano cells (Ta-
 236 ble S6 in Supplemental Information). Near the half of Orgnano and Orgpicopro SWUE
 237 abundance peaks exceeded their median bloom abundances (Table S7 in Supplemental
 238 Information). Besides, more than 4/5 of SWUEs saw Rednano, Redpicoeuk and Red-
 239 picopro abundances go higher than their respective median abundances during the spring
 240 bloom.

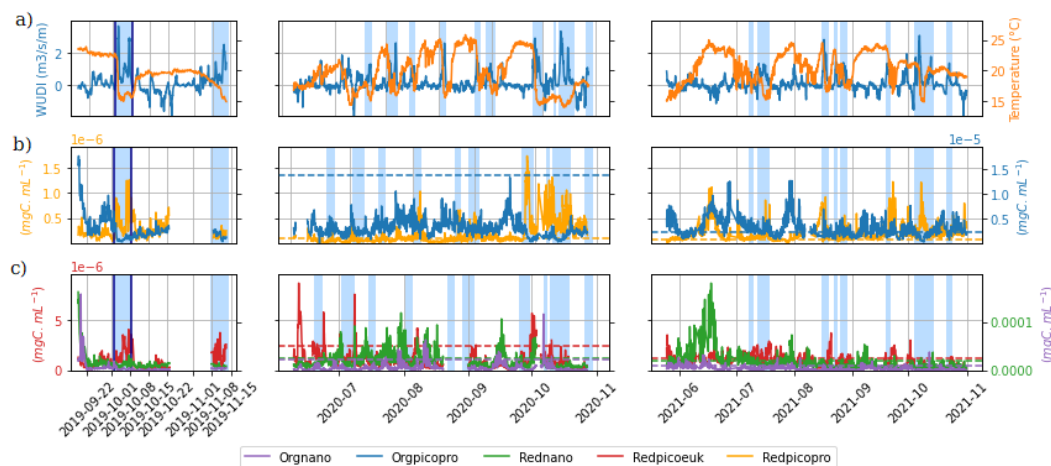


Figure 1. Time series of (a) Wind-driven Upwelling/Downwelling Index (WUDI, $m^3.s^{-1}m^{-1}$) and temperature ($^{\circ}C$) as well as (b, c) phytoplankton biomasses ($\mu gC.mL^{-1}$) monitored at the SSL@MM coastal station. The blue rectangles correspond to the 20 studied SWUEs. The event shown in Figure 2 is bounded by a dark blue box. The horizontal dashed colored lines correspond to the median biomasses observed during the spring bloom (except for 2019, not available) for each PFG (according to the color code).

241 **3.3 Characterization of the Phytoplankton Response: A Single Event** 242 **Illustration**

243 The typical effect of wind-induced upwellings on temperature and pico-nanophytoplankton
244 biomass is illustrated in Figure 2, showing differentiated responses among the PFGs. This
245 event was fueled by three periods of intense wind forcings, or intensification periods, that
246 generated an abrupt drop in temperature (-7.6°C) followed by the maintenance of cold
247 waters for six days. As shown in Figure S6 in Supplemental Information, during these
248 three sub-events, the N/P ratio rose after each wind intensification with a short delay,
249 especially after the third one that multiplied the nitrates, nitrites, and phosphates con-
250 centration by a factor of 19, 5, and 5, respectively.

251 The biomass reactions of the Redpicopro, Orgpicopro, and Orgnano groups to this
252 SWUE were quasi-instantaneous while they appeared after a short delay for the Red-
253 picoeuk and Rednano cells (~ 3 days). The biomass reaction magnitude was $+42.7\%$ for
254 the Rednano, $+123.7\%$ for the Orgnano, $+178.7\%$ for the Redpicoeuk, $+377.3\%$ for the
255 Redpicopro, and -82.1% for the Orgpicopro. Biomass levels decreased in the relaxation
256 phase for all PFGs except the Orgnano.
257 The estimated hourly growth rates (Figure S7 in Supplemental Information) varied in-
258 versely with respect to the biomass (Figure 2) and the abundance (data not shown): when
259 the PFG was high in biomass, its growth rate was estimated to be low and conversely.

260 **3.4 Detailed Characterization of the Phytoplankton Response**

261 The PFG abundances showed reaction delays ranging between 24h and 36h in me-
262 dian (Figure 3a). The reaction duration of the PFGs lasted between three and four days
263 in median, with a lower Inter-Quartile Range (IQR)/median ratio than the reaction de-
264 lay (Figure 3e). Concerning the reaction magnitude, the Orgnano and Orgpicopro abun-
265 dances decreased while the other PFGs generally saw their abundances rising (Figure
266 3c). The Redpicopro and Redpicoeuk presented the largest increases in abundance. Their
267 large IQRs were explained by some intense positive reactions for the majority of the SWUEs
268 while only five presented moderately negative reactions for both groups. The abundance
269 levels in the relaxation period decreased for all PFGs with median variations ranging from
270 -28.96% to -52.85% (Figure 3g).

271 In terms of biomass, the Orgpicopro reacted in less than one day, the Orgnano and
272 Redpicopro in less than two days, and Rednano and Redpicoeuk median reaction delay
273 was three days (Figure 3b). The majority of reaction durations lasted between two and
274 five days (Figure 3f). The signs of the reactions remained the same as for the abundance,
275 except for the Orgnano that experienced a positive biomass reaction (Figure 3d). In the
276 relaxation periods, the biomass levels decreased for all PFGs (-27.58% to -61.90% in me-
277 dian). However, positive relaxation magnitudes were observed in five SWUEs both for
278 Orgpicopro and Rednano, explaining higher variance than for other PFGs (Figure 3h).

279 The estimated growth rates of the PFGs tended to slow down during the reaction
280 phase and then increase during the relaxation phase (Figure S8 in Supplemental Infor-
281 mation), except for the Orgpicopro. This pattern was however significant for Redpicoeuk
282 cells only (Kruskal-Wallis test, $p\text{-value} \leq 0.01$).

283 **4 Discussion**

284 The Bay of Marseille located in the NW Mediterranean upwelling system is a nat-
285 ural laboratory to explore the impact of wind-driven coastal processes on oligotrophic
286 communities because of the unique intensities and short duration of upwelling events (Odic
287 et al., 2022). During the stratified periods, the SWUEs had a clear signature on the sea-
288 water surface temperature. The expected signature on nutrient enrichment was less sig-

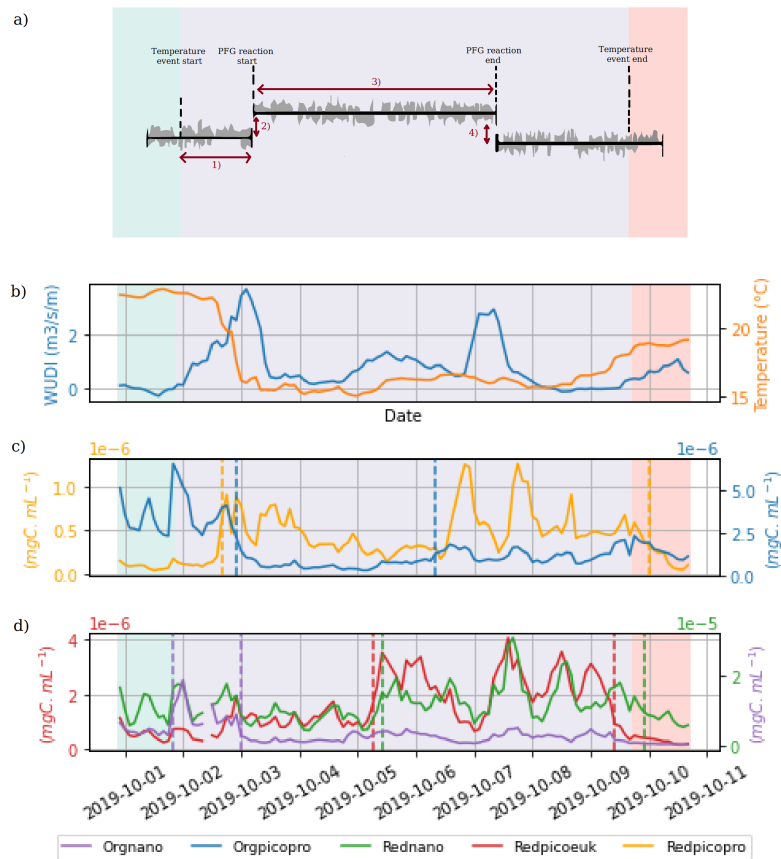


Figure 2. Illustrative view of a typical SWUE (highlighted by a dark blue box in Figure 1).

a) Characterisation of the biological response to an SWUE. The grey-shaded time series represents a schematic PFG time series and the background shading corresponds to the temperature anomaly phases defining the physical event: pre-anomaly (green), anomaly (violet), and post-anomaly phase (red). The characterization is performed using four attributes: (1) the reaction delay, (2) the reaction magnitude, (3) the reaction duration, (4) and the relaxation magnitude. b) Variation of the WUDI ($m^3 \cdot s^{-1} m^{-1}$, blue line) and the temperature ($^{\circ}C$, orange line), c) Biomass ($mgC \cdot mL^{-1}$) of Redpicopro and Orgpicopro d) Biomass ($mgC \cdot mL^{-1}$) of Redpicoeuk, Rednano, and Orgnano. The vertical dashed lines represent the ruptures automatically detected by the statistical method for each PFG, according to the color code.

289 significant, probably due to the littoral conditions, the delay needed for upwelled nutrients
 290 to reach the surface sampling point (e.g. nutrient consumption during the advection from
 291 the upwelling exit point to the sampling point), but also largely to the low and irregu-
 292 lar nutrient sampling rates (see Figure S3 in Supplemental Information).

293 As mentioned in García-Reyes et al. (2014), Rossi et al. (2014), and Armbrrecht et
 294 al. (2014), the physically-driven temperature drops and nutrient enrichments are key in-
 295 dicators to characterize the impact of SWUEs over the phytoplankton community. Us-
 296 ing a statistical rupture detection method, the causal effects of the environmental shifts
 297 over the pico-nanophytoplankton functional groups were assessed, capturing more than
 298 simple correlations and evidencing differentiated response patterns.

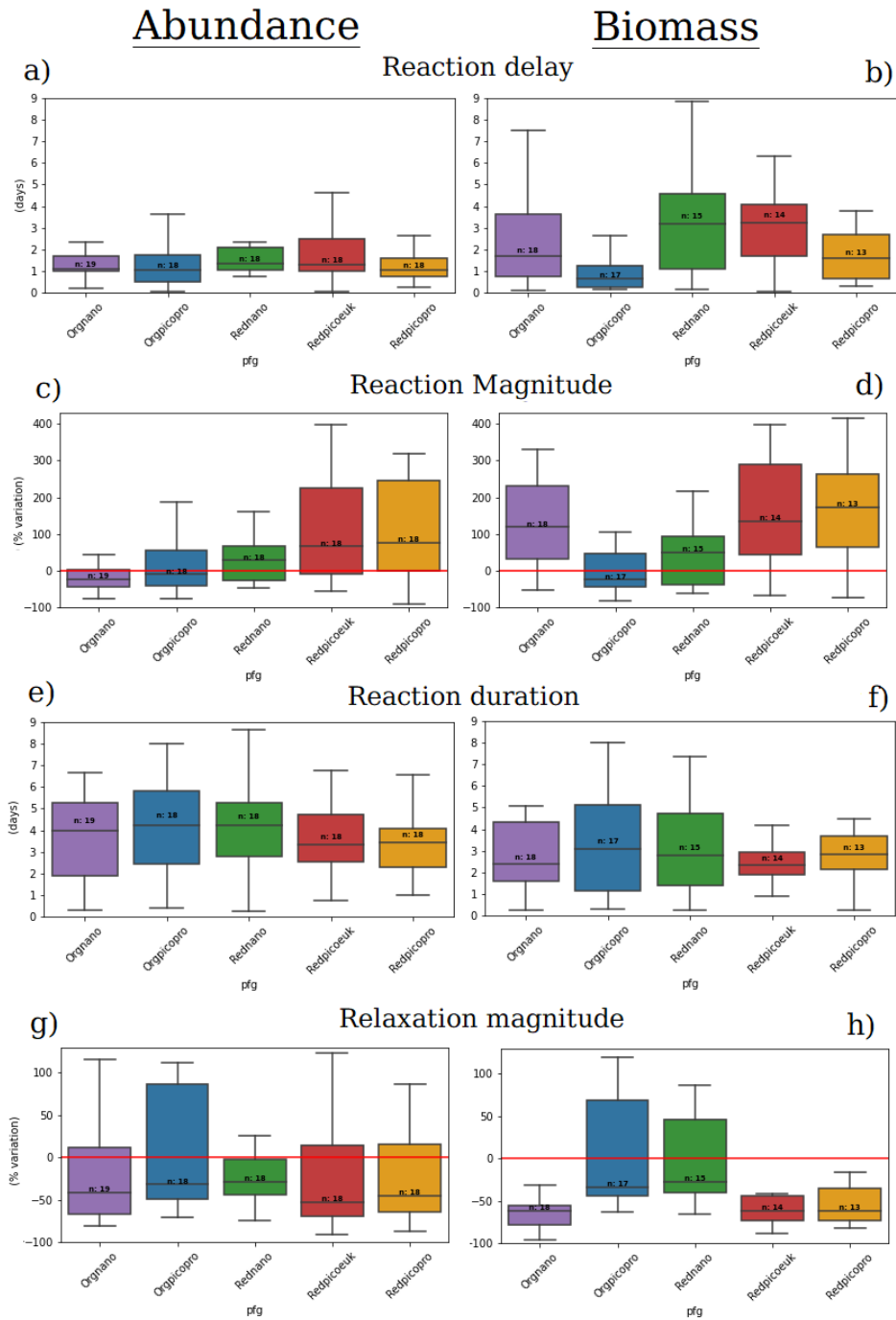


Figure 3. Boxplots of the reaction delay (a and b), the reaction magnitude (c and d), the reaction duration (e and f) and the relaxation magnitude (g and h) in terms of abundance and biomass, respectively, for five different PFGs. The horizontal red lines represent a variation of 0%. *n* denotes the number of SWUE for each PFG on which the boxplot has been constructed.

299 The phytoplankton functional groups reacted to the SWUEs in one to five days,
 300 a delay consistent with several studies evidencing phytoplankton biomass peaks two to
 301 five days after nutrient enrichment (Edwards et al., 2005; Hauss et al., 2012; Teixeira et

302 al., 2018). Certainly also fostered by surface higher light availability, the reaction du-
303 rations lasted between two and five days and were positive for all PFG abundances ex-
304 cept for the Orgnano and Orgpicopro cells and for all PFG biomasses except for the Org-
305 picopro cells. The comparison with previous studies is complicated by the different phy-
306 toplankton nomenclatures used. For instance, as both Orgpicopro and Redpicopro are
307 cyanobacteria, it is difficult to match the decrease in Orgpicopro and increase in Red-
308 picopro evidenced here with the increase in cyanobacteria observed by Martin-Platero
309 et al. (2018). Yet, the joint Redpicopro abundance positive reaction and increase in N/P
310 ratio during the event is consistent with Martiny et al. (2016). Similarly, the co-occurrence
311 of strong biological and N/P variability is in accordance with (Martz et al., 2014). The
312 negative sign of Orgnano reaction could be compared to the curbing abundance of cluster
313 C5 identified in Dugenne et al. (2014) after a wind event. Similarly, Thyssen et al.
314 (2008) have shown that two groups that presented similar red fluorescence/yellow flu-
315 orescence profiles as the Orgpicopro and Orgnano groups reacted differently than the other
316 functional groups to the SWUEs.

317 After the reaction, the PFGs presented mostly negative relaxation patterns except
318 for Orgpicopro and Orgnano during some SWUEs. As presented in Figure S9 in Sup-
319 plemental Information, there seems to exist an inverse relationship between these two
320 phases for most PFG abundances and biomasses: the more positive the reaction was, the
321 more negative the relaxation will be for a given PFG. This can be interpreted as envi-
322 ronmental forces pushing back to the steady state. These forces remain however to be
323 identified and could be of various nature: nutrient depletion (Wilkerson et al., 2006), com-
324 petition between functional groups (Martin-Platero et al., 2018), viral lysis or predation
325 (Sun et al., 2007; Coello-Camba et al., 2020). Following Hunter-Cevera et al. (2014), the
326 effect of these forces can be estimated using the model loss, i.e. the difference between
327 the observed PFG population growth rates and their estimations by the size-structured
328 model. The authors showed that the more correlated the loss is to the growth rate, the
329 more likely these losses are caused by biological factors. As made visible in Figure S10
330 in Supplemental Information, only the Rednana and Orgnana losses were significantly
331 but weakly correlated ($r \leq 0.31$) with their growth rates in the relaxation phase. These
332 low or non-significant correlations between growth rates and PFG losses seem to indi-
333 cate that physical forces, such as water masses switches, or water column re-stratification,
334 as well as biogeochemical hindrances (e.g. nutrient depletion or co-limitation) are dom-
335 inant during this phase as compared with grazing and viral lysis.

336 The PFG responses have been characterized thanks to a fine temporal and functional-
337 level resolution. As evoked in Martin-Platero et al. (2018), the chosen taxonomic level
338 (taxa, genera, etc.) along with the temporal frequency have a strong impact on the re-
339 sponse patterns observed (see also Figure S11 in Supplemental Information). In their stud-
340 ies, Martin-Platero et al. (2018) have used Operational taxonomic units (OTUs) based
341 on rRNA sequences similarity, while Martiny et al. (2016) relied on functional groups
342 close to the ones of this study obtained using diagnostic pigments. We used automated
343 pulse-shape recording flow cytometry to obtain an infra-day resolution over a long pe-
344 riod and a resolution up to the cytometric functional group. Each functional group con-
345 tains several ecotypes which could affect the estimated growth rates (Hunter-Cevera et
346 al., 2014) and add uncertainty to the size-structured model. The effect of complete PFG
347 population replacements that could occur during extremely strong SWUEs may addi-
348 tionally impact the presented estimations. This is also the case of the independence be-
349 tween predator behaviors and the phytoplankton cell sizes assumed by the model that
350 could not be tested here. As a result, the estimated growth rates were principally used
351 to give context to the underlying phenomena and to emphasize the fast and remarkable
352 impacts of SWUE on phytoplankton dynamics. Future research could hence use the in-
353 troduced high-frequency methodology to derive the proper impact of SWUE on phyto-
354 plankton primary production.

355 Similarly, while the temporal aspects of such tight biophysical coupled mechanisms
 356 are well-resolved by our sampling strategy and numerical approach, the present study
 357 did not offer a comprehensive view of the spatial variability at stake. When coupling physics
 358 with biology, the observed biological response of the PFGs could dramatically vary de-
 359 pending on whether the water masses were vertically originated (for example near the
 360 Deep Chlorophyll Maximum rather than near the seabed which would explain the lower
 361 nutrient variations than expected), or horizontally originated due to advection. The phy-
 362 toplankton biomass spatial dynamics, approached by chlorophyll-a concentration, have
 363 been extensively tracked by satellite (Wu et al., 2008; d’Ortenzio & Ribera d’Alcalà, 2009;
 364 Mayot et al., 2016; Lehahn et al., 2017; El Hourany et al., 2019), notably to evidence the
 365 “Dilution–Recoupling Hypothesis” that could have had an impact here (Behrenfeld, 2010).
 366 However, the satellites typically have issues resolving coastal areas and submesoscale pat-
 367 terns, focus on surface waters, have lower temporal resolutions (e.g. daily for sea sur-
 368 face temperature, weekly for clear chlorophyll-a maps) and hence could not properly re-
 369 solve the phytoplankton nycthemeral cycles.

370 In this respect, multi-year high-frequency in situ measurements, such as the ones
 371 performed at the SSL@MM coastal laboratory, could bring crucial missing pieces of in-
 372 formation. It could for instance be complementary to the work of Alvain et al. (2008)
 373 that matched chlorophyll-a anomalies resolved by satellite with phytoplankton commu-
 374 nity structures collected in situ. Other methods such as autonomous vehicle fleets (Jaffe
 375 et al., 2017), coastal radars (HFRs) (Cianelli et al., 2017), or 3D models coupling physics
 376 and biogeochemistry (Frayse et al., 2013) could be used jointly with the SSL@MM data
 377 to gain further insights about spatial dynamics and help guide future modeling efforts.

378 In summary, the SWUEs have generated significant abundance and biomass responses
 379 from the pico-nanophytoplankton community. From our data, the biggest total biomass
 380 increase due to a single wind-induced upwelling represented 5.3% of the total spring bloom
 381 biomass increase (due to its short duration) but 97.6% of the daily biomass increase im-
 382 putable to the spring bloom. This emphasizes that these events occurring several times
 383 a year are intense and significantly impact the seasonal dynamics and annual carbon bud-
 384 get. The consistent time scales and magnitudes of biological responses reported here for
 385 sporadic wind-induced events using an innovative sampling strategy and an advanced
 386 statistical methodology could provide new insights on how to observe, and perhaps model,
 387 the impact of other submesoscale events on phytoplankton communities.

388 **Acknowledgments**

389 The authors are grateful to Cytobuoy b.v. for the personalized software developments
 390 performed on the CytoClus4© software features. At the SSL@MM station, the data could
 391 not have been collected without the support of Michel Durand, the MIO Service Atmo-
 392 sphere Mer (Deny Malengros and Fabrice Garcia), and UMS OSU Pytheas (Christian
 393 Marshal and Dorian Guillemain) that maintain the pumping inlet. Additional support
 394 for the SSL@MM was provided by Aix Marseille Université, MIO, and OSU PYTHEAS.
 395 The authors are also very thankful to Ivane Pairaud and the team exploiting the MESURHO
 396 buoy (Cadiou et al., 2010) for the PAR data, and to the MIO-PACEM platform for the
 397 nutrients analysis. Funding for R.F.’s Ph.D. thesis was provided by the Ministry of Higher
 398 Education, Research, and Innovation. The project leading to this publication has received
 399 funding from the ERDF under project 1166-39417. The project leading to this publi-
 400 cation has received funding from the Excellence Initiative of Aix-Marseille University -
 401 A*MIDEX, a French “Investissements d’Avenir” program. V.R., N.B. and C.P. acknowl-
 402 edge financial support from the European Commission through the programme “Car-
 403 oline Herschel” (FPACUP_SGA4_Tier1; agreement number: 2020/SI.2.833213) through
 404 the project entitled “Developing Downstream applications and services on BIO-PHYsical
 405 characterization of the seascape for COASTal management (BIOPHYCOAST)

Open Research

The code and data to reproduce the presented results of the paper are available at <https://github.com/RobeeF/PhytoUpwellingPaper>.

The associated DOI is <https://doi.org/10.5281/zenodo.6626707>

References

- Alvain, S., Moulin, C., Dandonneau, Y., & Loisel, H. (2008). Seasonal distribution and succession of dominant phytoplankton groups in the global ocean: A satellite view. *Global Biogeochemical Cycles*, *22*(3).
- Antoine, D., Morel, A., & André, J.-M. (1995). Algal pigment distribution and primary production in the eastern mediterranean as derived from coastal zone color scanner observations. *Journal of Geophysical Research: Oceans*, *100*(C8), 16193–16209.
- Armbrecht, L. H., Roughan, M., Rossi, V., Schaeffer, A., Davies, P. L., Waite, A. M., & Armand, L. K. (2014). Phytoplankton composition under contrasting oceanographic conditions: Upwelling and downwelling (eastern australia). *Continental Shelf Research*, *75*, 54–67.
- Bai, J., & Perron, P. (2003). Critical values for multiple structural change tests. *The Econometrics Journal*, *6*(1), 72–78.
- Bakun, A. (1973). Coastal upwelling indices, west coast of north america, 1946-71. *NOAA technical report*.
- Bakun, A., & Agostini, V. N. (2001). Seasonal patterns of wind-induced upwelling/downwelling in the mediterranean sea. *Scientia Marina*, *65*(3), 243–257.
- Bauer, J. E., Cai, W.-J., Raymond, P. A., Bianchi, T. S., Hopkinson, C. S., & Rignier, P. A. (2013). The changing carbon cycle of the coastal ocean. *Nature*, *504*(7478), 61–70.
- Behrenfeld, M. J. (2010). Abandoning sverdrup’s critical depth hypothesis on phytoplankton blooms. *Ecology*, *91*(4), 977–989.
- Bensoussan, N., Romano, J.-C., Harmelin, J.-G., & Garrabou, J. (2010). High resolution characterization of northwest mediterranean coastal waters thermal regimes: to better understand responses of benthic communities to climate change. *Estuarine, Coastal and Shelf Science*, *87*(3), 431–441.
- Bolaños, L. M., Karp-Boss, L., Choi, C. J., Worden, A. Z., Graff, J. R., Haëntjens, N., ... others (2020). Small phytoplankton dominate western north atlantic biomass. *The ISME journal*, *14*(7), 1663–1674.
- Borges, A. V., Delille, B., & Frankignoulle, M. (2005). Budgeting sinks and sources of co₂ in the coastal ocean: Diversity of ecosystems counts. *Geophysical research letters*, *32*(14).
- Bosc, E., Bricaud, A., & Antoine, D. (2004). Seasonal and interannual variability in algal biomass and primary production in the mediterranean sea, as derived from 4 years of seawifs observations. *Global Biogeochemical Cycles*, *18*(1).
- Brody, S. R., Lozier, M. S., & Dunne, J. P. (2013). A comparison of methods to determine phytoplankton bloom initiation. *Journal of Geophysical Research: Oceans*, *118*(5), 2345–2357.
- Cadiou, J.-F., Repecaud, M., Arnaud, M., Rabouille, C., Raimbaud, P., Radakovitch, O., ... Gaufrès, P. (2010). Mesurho: a high frequency oceanographic buoy at the rhone river mouth. In *39th ciesm congress-venice, italy, 10-14 may 2010*.
- Cianelli, D., D’Alelio, D., Uttieri, M., Sarno, D., Zingone, A., Zambianchi, E., & d’Alcalà, M. R. (2017). Disentangling physical and biological drivers of phytoplankton dynamics in a coastal system. *Scientific reports*, *7*(1), 1–15.
- Coello-Camba, A., Diaz-Rua, R., Duarte, C. M., Irigoien, X., Pearman, J. K., Alam,

- 458 I. S., & Agusti, S. (2020). Picocyanobacteria community and cyanophage
459 infection responses to nutrient enrichment in a mesocosms experiment in
460 oligotrophic waters. *Frontiers in Microbiology*, *11*, 1153. Retrieved from
461 <https://www.frontiersin.org/article/10.3389/fmicb.2020.01153> doi:
462 10.3389/fmicb.2020.01153
- 463 d’Ortenzio, F., & Ribera d’Alcalà, M. (2009). On the trophic regimes of the mediter-
464 ranean sea: a satellite analysis. *Biogeosciences*, *6*(2), 139–148.
- 465 Dubelaar, G. B., & Gerritzen, P. L. (2000). Cytobuoy: a step forward towards using
466 flow cytometry in operational oceanography. *Scientia Marina*, *64*(2), 255–265.
- 467 Dubelaar, G. B., Gerritzen, P. L., Beeker, A. E., Jonker, R. R., & Tangen, K.
468 (1999). Design and first results of cytobuoy: A wireless flow cytometer for
469 in situ analysis of marine and fresh waters. *Cytometry: The Journal of the*
470 *International Society for Analytical Cytology*, *37*(4), 247–254.
- 471 Dugenne, M., Thyssen, M., Nerini, D., Mante, C., Poggiale, J.-C., Garcia, N., ...
472 Grégori, G. J. (2014). Consequence of a sudden wind event on the dynamics of
473 a coastal phytoplankton community: an insight into specific population growth
474 rates using a single cell high frequency approach. *Frontiers in microbiology*, *5*,
475 485.
- 476 Edwards, V., Icely, J., Newton, A., & Webster, R. (2005). The yield of chlorophyll
477 from nitrogen: a comparison between the shallow ria formosa lagoon and the
478 deep oceanic conditions at sagres along the southern coast of portugal. *Estuar-*
479 *ine, Coastal and Shelf Science*, *62*(3), 391–403.
- 480 El Hourany, R., Abboud-abi Saab, M., Faour, G., Mejia, C., Crépon, M., & Thiria,
481 S. (2019). Phytoplankton diversity in the mediterranean sea from satellite data
482 using self-organizing maps. *Journal of Geophysical Research: Oceans*, *124*(8),
483 5827–5843.
- 484 Field, C. B., Behrenfeld, M. J., Randerson, J. T., & Falkowski, P. (1998). Primary
485 production of the biosphere: integrating terrestrial and oceanic components.
486 *science*, *281*(5374), 237–240.
- 487 Fraysse, M., Pinazo, C., Faure, V. M., Fuchs, R., Lazzari, P., Raimbault, P., &
488 Pairaud, I. (2013). Development of a 3d coupled physical-biogeochemical
489 model for the marseille coastal area (nw mediterranean sea): what complexity
490 is required in the coastal zone? *PloS one*, *8*(12), e80012.
- 491 Fuchs, R., Thyssen, M., Creach, V., Dugenne, M., Izard, L., Latimier, M., ... Pom-
492 meret, D. (2022). Automatic recognition of flow cytometric phytoplank-
493 ton functional groups using convolutional neural networks. *Limnology and*
494 *Oceanography: Methods*. doi: <https://doi.org/10.1002/lom3.10493>
- 495 García-Reyes, M., Largier, J. L., & Sydeman, W. J. (2014). Synoptic-scale up-
496 welling indices and predictions of phyto-and zooplankton populations. *Progress*
497 *in Oceanography*, *120*, 177–188.
- 498 Gattuso, J., Frankignoulle, M., & Wollast, R. (1998). Carbon and carbonate
499 metabolism in coastal aquatic ecosystems. *Annual Review of Ecology, Evo-*
500 *lution, and Systematics*, *29*, 405–434.
- 501 Grob, C., Ulloa, O., Claustre, H., Huot, Y., Alarcon, G., & Marie, D. (2007). Con-
502 tribution of picoplankton to the total particulate organic carbon concentration
503 in the eastern south pacific. *Biogeosciences*, *4*(5), 837–852.
- 504 Hauss, H., Franz, J. M., & Sommer, U. (2012). Changes in n: P stoichiometry in-
505 fluence taxonomic composition and nutritional quality of phytoplankton in the
506 peruvian upwelling. *Journal of sea Research*, *73*, 74–85.
- 507 Hunter-Cevera, K. R., Neubert, M. G., Olson, R. J., Shalapyonok, A., Solow, A. R.,
508 & Sosik, H. M. (2020). Seasons of syn. *Limnology and oceanography*, *65*(5),
509 1085–1102.
- 510 Hunter-Cevera, K. R., Neubert, M. G., Solow, A. R., Olson, R. J., Shalapyonok, A.,
511 & Sosik, H. M. (2014). Diel size distributions reveal seasonal growth dynamics
512 of a coastal phytoplankter. *Proceedings of the National Academy of Sciences*,

- 513 111 (27), 9852–9857.
- 514 Jaffe, J. S., Franks, P. J., Roberts, P. L., Mirza, D., Schurgers, C., Kastner, R., &
515 Boch, A. (2017). A swarm of autonomous miniature underwater robot drifters
516 for exploring submesoscale ocean dynamics. *Nature communications*, 8(1),
517 1–8.
- 518 Lajaunie-Salla, K., Diaz, F., Wimart-Rousseau, C., Wagener, T., Lefèvre, D., Yohia,
519 C., ... Pinazo, C. (2021). Implementation and assessment of a carbonate
520 system model (eco3m-carbox v1. 1) in a highly dynamic mediterranean coastal
521 site (bay of marseille, france). *Geoscientific Model Development*, 14(1), 295–
522 321.
- 523 Lehahn, Y., Koren, I., Sharoni, S., d’Ovidio, F., Vardi, A., & Boss, E. (2017). Dis-
524 persion/dilution enhances phytoplankton blooms in low-nutrient waters. *Na-
525 ture Communications*, 8(1), 1–8.
- 526 Lévy, M., Ferrari, R., Franks, P. J., Martin, A. P., & Rivière, P. (2012). Bringing
527 physics to life at the submesoscale. *Geophysical Research Letters*, 39(14).
- 528 Li, W. (1995). Composition of ultraphytoplankton in the central north atlantic. *Ma-
529 rine Ecology Progress Series*, 122, 1–8.
- 530 Lomas, M. W., & Moran, S. B. (2011). Evidence for aggregation and export of
531 cyanobacteria and nano-eukaryotes from the sargasso sea euphotic zone. *Bio-
532 geosciences*, 8(1), 203–216.
- 533 Lomas, M. W., Roberts, N., Lipschultz, F., Krause, J., Nelson, D., & Bates, N.
534 (2009). Biogeochemical responses to late-winter storms in the sargasso sea. iv.
535 rapid succession of major phytoplankton groups. *Deep Sea Research Part I:
536 Oceanographic Research Papers*, 56(6), 892–908.
- 537 Marrec, P., Grégori, G., Doglioli, A. M., Dugenne, M., Della Penna, A., Bhairy,
538 N., ... Thyssen, M. (2018). Coupling physics and biogeochemistry thanks
539 to high-resolution observations of the phytoplankton community structure in
540 the northwestern mediterranean sea. *Biogeosciences*, 15(5), 1579–1606. Re-
541 trieved from <https://bg.copernicus.org/articles/15/1579/2018/> doi:
542 10.5194/bg-15-1579-2018
- 543 Martin-Platero, A. M., Cleary, B., Kauffman, K., Preheim, S. P., McGillicuddy,
544 D. J., Alm, E. J., & Polz, M. F. (2018). High resolution time series reveals
545 cohesive but short-lived communities in coastal plankton. *Nature communica-
546 tions*, 9(1), 1–11.
- 547 Martiny, A. C., Talarmin, A., Mouginot, C., Lee, J. A., Huang, J. S., Gellene, A. G.,
548 & Caron, D. A. (2016). Biogeochemical interactions control a temporal suc-
549 cession in the elemental composition of marine communities. *Limnology and
550 Oceanography*, 61(2), 531–542.
- 551 Martz, T., Send, U., Ohman, M. D., Takeshita, Y., Bresnahan, P., Kim, H.-J., &
552 Nam, S. (2014). Dynamic variability of biogeochemical ratios in the southern
553 california current system. *Geophysical Research Letters*, 41(7), 2496–2501.
- 554 Mayot, N., d’Ortenzio, F., Ribera d’Alcalà, M., Lavigne, H., & Claustre, H. (2016).
555 Interannual variability of the mediterranean trophic regimes from ocean color
556 satellites. *Biogeosciences*, 13(6), 1901–1917.
- 557 Menden-Deuer, S., & Lessard, E. J. (2000). Carbon to volume relationships for di-
558 noflagellates, diatoms, and other protist plankton. *Limnology and oceanogra-
559 phy*, 45(3), 569–579.
- 560 Millot, C. (1979). Wind induced upwellings in the gulf of lions. *Oceanologica Acta*,
561 2(3), 261–274.
- 562 Morel, A., & André, J.-M. (1991). Pigment distribution and primary production
563 in the western mediterranean as derived and modeled from coastal zone color
564 scanner observations. *Journal of Geophysical Research: Oceans*, 96(C7),
565 12685–12698.
- 566 Odic, R., Bensoussan, N., Pinazo, C., Taupier-Letage, I., & Rossi, V. (2022). Spo-
567 radic wind-driven upwelling/downwelling and associated cooling/warming

- 568 along northwestern mediterranean coastlines. *Continental Shelf Research*
 569 *(accepted)*.
- 570 Olson, R. J., Shalapyonok, A., & Sosik, H. M. (2003). An automated submersible
 571 flow cytometer for analyzing pico-and nanophytoplankton: Flowcytobot. *Deep*
 572 *Sea Research Part I: Oceanographic Research Papers*, 50(2), 301–315.
- 573 Pairaud, I., Gatti, J., Bensoussan, N., Verney, R., & Garreau, P. (2011). Hydrology
 574 and circulation in a coastal area off marseille: Validation of a nested 3d model
 575 with observations. *Journal of marine systems*, 88(1), 20–33.
- 576 Palma, E. D., & Matano, R. P. (2009). Disentangling the upwelling mechanisms of
 577 the south brazil bight. *Continental Shelf Research*, 29(11-12), 1525–1534.
- 578 Ribalet, F., Swalwell, J., Clayton, S., Jiménez, V., Sudek, S., Lin, Y., . . . Armbrust,
 579 E. V. (2015). Light-driven synchrony of prochlorococcus growth and mortal-
 580 ity in the subtropical pacific gyre. *Proceedings of the National Academy of*
 581 *Sciences*, 112(26), 8008–8012.
- 582 Richardson, T. L., & Jackson, G. A. (2007). Small phytoplankton and carbon export
 583 from the surface ocean. *Science*, 315(5813), 838–840.
- 584 Rossi, V., Garçon, V., Tassel, J., Romagnan, J.-B., Stemmann, L., Jourdin, F., . . .
 585 Morel, Y. (2013). Cross-shelf variability in the iberian peninsula upwelling sys-
 586 tem: Impact of a mesoscale filament. *Continental Shelf Research*, 59, 97–114.
- 587 Rossi, V., Schaeffer, A., Wood, J., Galibert, G., Morris, B., Sudre, J., . . . Waite,
 588 A. M. (2014). Seasonality of sporadic physical processes driving tempera-
 589 ture and nutrient high-frequency variability in the coastal ocean off southeast
 590 australia. *Journal of Geophysical Research: Oceans*, 119(1), 445–460.
- 591 Sapiano, M., Brown, C., Schollaert Uz, S., & Vargas, M. (2012). Establishing a
 592 global climatology of marine phytoplankton phenological characteristics. *Jour-*
 593 *nal of Geophysical Research: Oceans*, 117(C8).
- 594 Sosik, H. M., Olson, R. J., Neubert, M. G., Shalapyonok, A., & Solow, A. R. (2003).
 595 Growth rates of coastal phytoplankton from time-series measurements with a
 596 submersible flow cytometer. *Limnology and Oceanography*, 48(5), 1756–1765.
- 597 Sun, J., Feng, Y., Zhang, Y., & Hutchins, D. (2007, 09). Fast microzooplankton
 598 grazing on fast-growing, low-biomass phytoplankton: A case study in spring in
 599 chesapeake bay, delaware inland bays and delaware bay. *Hydrobiologia*, 589,
 600 127–139. doi: 10.1007/s10750-007-0730-6
- 601 Sun, J., & Liu, D. (2003). Geometric models for calculating cell biovolume and sur-
 602 face area for phytoplankton. *Journal of plankton research*, 25(11), 1331–1346.
- 603 Teixeira, I., Arbones, B., Froján, M., Nieto-Cid, M., Álvarez-Salgado, X. A., Cas-
 604 tro, C. G., . . . Figueiras, F. (2018). Response of phytoplankton to enhanced
 605 atmospheric and riverine nutrient inputs in a coastal upwelling embayment.
 606 *Estuarine, Coastal and Shelf Science*, 210, 132–141.
- 607 Thyssen, M., Fuchs, R., Créach, V., Artigas, L. F., Grégori, G., Marrec, P., . . . oth-
 608 ers (2021). Standard vocabulary, consensual functional groups and automated
 609 classification for phytoplankton high throughput datasets using automated flow
 610 cytometry. In *Aslo 2021*.
- 611 Thyssen, M., Mathieu, D., Garcia, N., & Denis, M. (2008). Short-term variation of
 612 phytoplankton assemblages in mediterranean coastal waters recorded with an
 613 automated submerged flow cytometer. *Journal of Plankton Research*, 30(9),
 614 1027–1040.
- 615 Tréguer, P., & Le Corre, P. (1975). Manuel d’analyse des sels nutritifs dans l’eau de
 616 mer (utilisation de l’autoanalyseur ii technicon), 110, lab. d’océanogr. *Chim.,*
 617 *Univ. de Bretagne Occident., Brest, France*.
- 618 Truong, C., Oudre, L., & Vayatis, N. (2020). Selective review of offline change point
 619 detection methods. *Signal Processing*, 167, 107299.
- 620 Verity, P. G., Robertson, C. Y., Tronzo, C. R., Andrews, M. G., Nelson, J. R., &
 621 Sieracki, M. E. (1992). Relationships between cell volume and the carbon
 622 and nitrogen content of marine photosynthetic nanoplankton. *Limnology and*

- 623 *Oceanography*, 37(7), 1434–1446.
- 624 Wilkerson, F. P., Lassiter, A. M., Dugdale, R. C., Marchi, A., & Hogue, V. E.
625 (2006). The phytoplankton bloom response to wind events and upwelled
626 nutrients during the coop west study. *Deep Sea Research Part II: Topical*
627 *Studies in Oceanography*, 53(25-26), 3023–3048.
- 628 Wimart-Rousseau, C., Lajaunie-Salla, K., Marrec, P., Wagener, T., Raimbault, P.,
629 Lagadec, V., . . . others (2020). Temporal variability of the carbonate system
630 and air-sea co₂ exchanges in a mediterranean human-impacted coastal site.
631 *Estuarine, Coastal and Shelf Science*, 236, 106641.
- 632 Wu, Y., Platt, T., Tang, C. C., Sathyendranath, S., Devred, E., & Gu, S. (2008). A
633 summer phytoplankton bloom triggered by high wind events in the labrador
634 sea, july 2006. *Geophysical Research Letters*, 35(10).